



Cellulose II Aerogel-Based Triboelectric Nanogenerator

Lei Zhang, Yang Liao, Yi-Cheng Wang,* Steven Zhang, Weiqing Yang, Xuejun Pan,* and Zhong Lin Wang*

Cellulose-based triboelectric nanogenerators (TEGs) have gained increasing attention. In this study, a novel method is demonstrated to synthesize cellulose-based aerogels and such aerogels are used to fabricate TEGs that can serve as mechanical energy harvesters and self-powered sensors. The cellulose II aerogel is fabricated via a dissolution–regeneration process in a green inorganic molten salt hydrate solvent (lithium bromide trihydrate), where. The as-fabricated cellulose II aerogel exhibits an interconnected open-pore 3D network structure, higher degree of flexibility, high porosity, and a high surface area of $221.3 \text{ m}^2 \text{ g}^{-1}$. Given its architectural merits, the cellulose II aerogel-based TENG presents an excellent mechanical response sensitivity and high electrical output performance. By blending with other natural polysaccharides, i.e., chitosan and alginic acid, electron-donating and electron-withdrawing groups are introduced into the composite cellulose II aerogels, which significantly improves the triboelectric performance of the TENG. The cellulose II aerogel-based TENG is demonstrated to light up light-emitting diodes, charge commercial capacitors, power a calculator, and monitor human motions. This study demonstrates the facile fabrication of cellulose II aerogel and its application in TENG, which leads to a high-performance and eco-friendly energy harvesting and self-powered system.

1. Introduction

Nature endows individuals with fulfilling all their requirements. Mechanical energy from the environment (e.g., wind,^[1] vibration,^[2] water,^[3] and human activities^[4]) represents a potential sustainable energy source that one could harvest. Triboelectric nanogenerator (TENG), derived from Maxwell's displacement current,^[5] can convert ambient distributed mechanical energy into electrical energy. Given the high power density, low cost, lightweight, and excellent manufacturability, TENG is highly promising in terms of addressing the energy supply required for the applications in distributed, mobile, disordered, and wired/wireless sites.^[6] However, the typical materials utilized in TENG are usually synthetic polymers such as polytetrafluoroethylene (PTFE), fluorinated ethylene, polyethylene terephthalate, and polydimethylsiloxane, which are nonrenewable and nonsustainable. Thus, it is attractive to implement renewable natural polymers in TENG.

Cellulose is a linear polymer composed of glucose units linked by $\beta(1,4)$ -glycosidic bond, and it is widely involved in almost every field of our daily life.^[7] It features numerous advantages, such as renewability, sustainability, biocompatibility, and biodegradability. Previous studies have employed cellulose to develop TENGs in lieu of other synthetic polymers in recent years, yet most of the work reported used cellulose-based films to assemble TENGs.^[8] Aerogel, with merits of low density, highly porous network structure, and high specific surface area,^[9] could provide superior electrical performance compared to film counterparts in TENG application.^[17] The prior reported cellulose-based aerogels for TENG were fabricated mostly from cellulose nanocrystal (CNC),^[8a,c] bacterial cellulose,^[8d] and cellulose nanofibril (CNF).^[10] These aerogels from CNC and CNF are usually brittle and less flexible, and have weak physical strength and low specific surface area, which could affect the fabrication and performance of TENG, as further discussed in the following section.

In the present study, we report a new approach to fabricate cellulose aerogels and their application in TENG for mechanical energy harvesters and self-powered sensors. The cellulose aerogels were fabricated via a process of dissolution and regeneration using inorganic molten salt hydrate

Dr. L. Zhang, S. Zhang, Prof. Z. L. Wang
School of Materials Science and Engineering
Georgia Institute of Technology
Atlanta, GA 30332-0245, USA
E-mail: zhong.wang@mse.gatech.edu

Dr. L. Zhang, Prof. W. Yang
Key Laboratory of Advanced Technologies of Materials
(Ministry of Education)
School of Materials Science and Engineering
Southwest Jiaotong University
Chengdu, Sichuan 610031, P. R. China

Dr. Y. Liao, Prof. X. Pan
Department of Biological Systems Engineering
University of Wisconsin-Madison
460 Henry Mall, Madison, WI 53706, USA
E-mail: xpan@wisc.edu

Prof. Y.-C. Wang
Department of Food Science and Human Nutrition
University of Illinois at Urbana-Champaign
Urbana, IL 61801, USA
E-mail: ycw@illinois.edu

The ORCID identification number(s) for the author(s) of this article can be found under <https://doi.org/10.1002/adfm.202001763>.

DOI: 10.1002/adfm.202001763

(lithium bromide trihydrate) as a new solvent, during which native cellulose (cellulose I) was converted to regenerated cellulose (cellulose II). This is why the aerogel fabricated by this approach is called cellulose II aerogel. Because of the unique gelation mechanism of this fabrication process, as discussed later, the cellulose II aerogel has a large number of mesopores generated by the solubilization–regeneration process; thereby, it has a larger surface area, which could significantly improve the TENGs' performance.^[11] In addition, the cellulose II aerogels are more flexible, stronger, and tougher than the ones from CNC and CNF because a continuous network structure of cellulose fibers was homogeneously formed during the fabrication of cellulose II aerogel. Therefore, the cellulose II aerogel-based TENG is expected to have excellent mechanical response sensitivity and high electrical output. Moreover, through blending with other natural polysaccharides to introduce electron-donating and electron-withdrawing groups, we fabricated a series of cellulose II aerogels with various tribopolarity, which is expected to greatly improve the electrical performance of TENGs. With the merits of the material and structure, the cellulose II aerogel-based TENG provides a green, effective, and a low-cost way for high-performance and eco-friendly energy harvesting and self-powered sensing systems.

2. Results and Discussions

2.1. Fabrication and Characterization of Cellulose II Aerogel

To prepare cellulose II materials, one must solubilize native cellulose and then regenerate it. However, the highly crystalline structure due to its strong inter- and intramolecular hydrogen bonds makes cellulose insoluble in common solvents, and only limited specific solvent systems can dissolve cellulose.^[12] Among them is inorganic molten salt hydrate (a concentrated aqueous solution of certain inorganic salts).^[13] Recently, lithium bromide trihydrate ($\text{LiBr} \cdot 3\text{H}_2\text{O}$, a molten salt hydrate) was found to be able to dissolve cellulose.^[14] The dissolution mechanism of cellulose in $\text{LiBr} \cdot 3\text{H}_2\text{O}$ can be briefly explained as follows. When LiBr is dissolved in water, Li^+ ions are coordinated or hydrated by water molecules, and the resultant hydrated lithium cations can coordinate with the hydroxyl groups of the cellulose, which disrupts the intermolecular hydrogen bond ($\text{O}(6)\text{H} \cdots \text{O}(3)$) and thereby facilitates the dissolution of cellulose. In addition, the free Br^- ions in the system accelerate the dissolution of cellulose by either promoting the $\text{Li}-\text{OH}$ coordination or directly interacting with cellulose– OH .

Figure 1a depicts the fabrication of cellulose II aerogel using lithium bromide trihydrate ($\text{LiBr} \cdot 3\text{H}_2\text{O}$) as a solvent. Cellulose was quickly dissolved in $\text{LiBr} \cdot 3\text{H}_2\text{O}$ under mild conditions to form a solution. Once cooled to room temperature, the solution directly gelled into a soft matter with a shape of its container, and this process required no antisolvent.^[15] After washing, the dissolved cellulose regenerated and aggregated into cellulose fibers that physically entangled each other and formed a monolithic piece of hydrogel, which was transparent in the water dispersion medium. After solvent exchanging and freeze-drying, the hydrogel was converted to cellulose II aerogel, which inherited its original shape and did not shrink (Figure 1b).

The scanning electron microscope (SEM) images in Figure 1c show the uniform network structure and porous fiber surface of the cellulose II aerogel. The layer-by-layer reconstruction of X-ray nano-computed tomography (nano-CT) further verifies the interconnected open-pore 3D network and uniform mass distribution (Figure 1d) of the aerogel. The rough surface of regenerated cellulose fibers significantly increases the surface area, resulting from a large amount of mesosized pores formed during the regeneration process.^[15b] The nitrogen adsorption–desorption test indicates that the Brunauer–Emmett–Teller (BET) surface area of the aerogel is $221.3 \text{ m}^2 \text{ g}^{-1}$, which is much larger than that of the previously reported cellulose I aerogel film ($68 \text{ m}^2 \text{ g}^{-1}$).^[10b] The Barrett–Joyner–Halenda (BJH) pore size distribution falls in the diameter range of 10–25 nm, suggesting that the cellulose II aerogel is a typical mesoporous material, based on the classification of International Union of Pure and Applied Chemistry.^[16]

Strain sweep test results (Figure 1e; Figure S1, Supporting Information) indicate that the cellulose II aerogel is a flexible material. Under stress, the cellulose II aerogel deformed, but did not fracture or crack due to the homogeneous interconnection structure. Besides, thermogravimetric analysis (Figure 1f) indicates that the cellulose II aerogel exhibited good thermal stability up to $250 \text{ }^\circ\text{C}$. The small mass loss below $100 \text{ }^\circ\text{C}$ was due to the evaporation of moisture absorbed by the hydrophilic cellulose.

The evidence above indicates that the as-prepared cellulose II aerogel is less rigid and more flexible, which would benefit the performance and durability of the TENGs. The advantages resulted from the dissolution–regeneration fabrication procedures, which led to a different aerogel structure from the aerogels made from cellulose I materials, such as CNC and CNF. CNC is highly crystallized and rigid cellulose rod with the length ranging from hundreds of nanometers to several micrometers.^[15a] A typical procedure for fabricating CNC-based aerogel is suspending CNC in water followed by freeze-drying, which aggregates CNC rods together to form a network matrix. The resultant aerogel is usually brittle and easily collapses under pressure because the force sustaining the network structure is mainly from the hydrogen bonding and van der Waals force between the CNC rods, which is much weaker than the strength of the rods themselves. As a result, the joints (bindings) between the CNC rods become the weakest points in the network, which leads to the fragile aerogel. CNF is longer and flexible, and thereby able to form more physical entanglement than CNC, which improves aerogel flexibility, but CNF-based aerogels still have similar drawbacks of the weak joints. CNC- or CNF-based aerogels are usually pressed into a film for the applications requiring strong mechanical strength. Chemical modification and crosslinking are additional strategies to further improve the mechanical property of CNC- and CNF-based aerogels.^[17] Differently, the cellulose II aerogel was prepared via a dissolution–regeneration process, in which cellulose was completely dissolved and then regenerated into a continuous and homogeneous network of cellulose fibers (Figure 1c,d) without the apparent weak joints as those in CNC or CNF aerogels. Therefore, the cellulose II aerogel is softer, more flexible, and tougher in response to applied pressure, which is desirable for TENG applications.

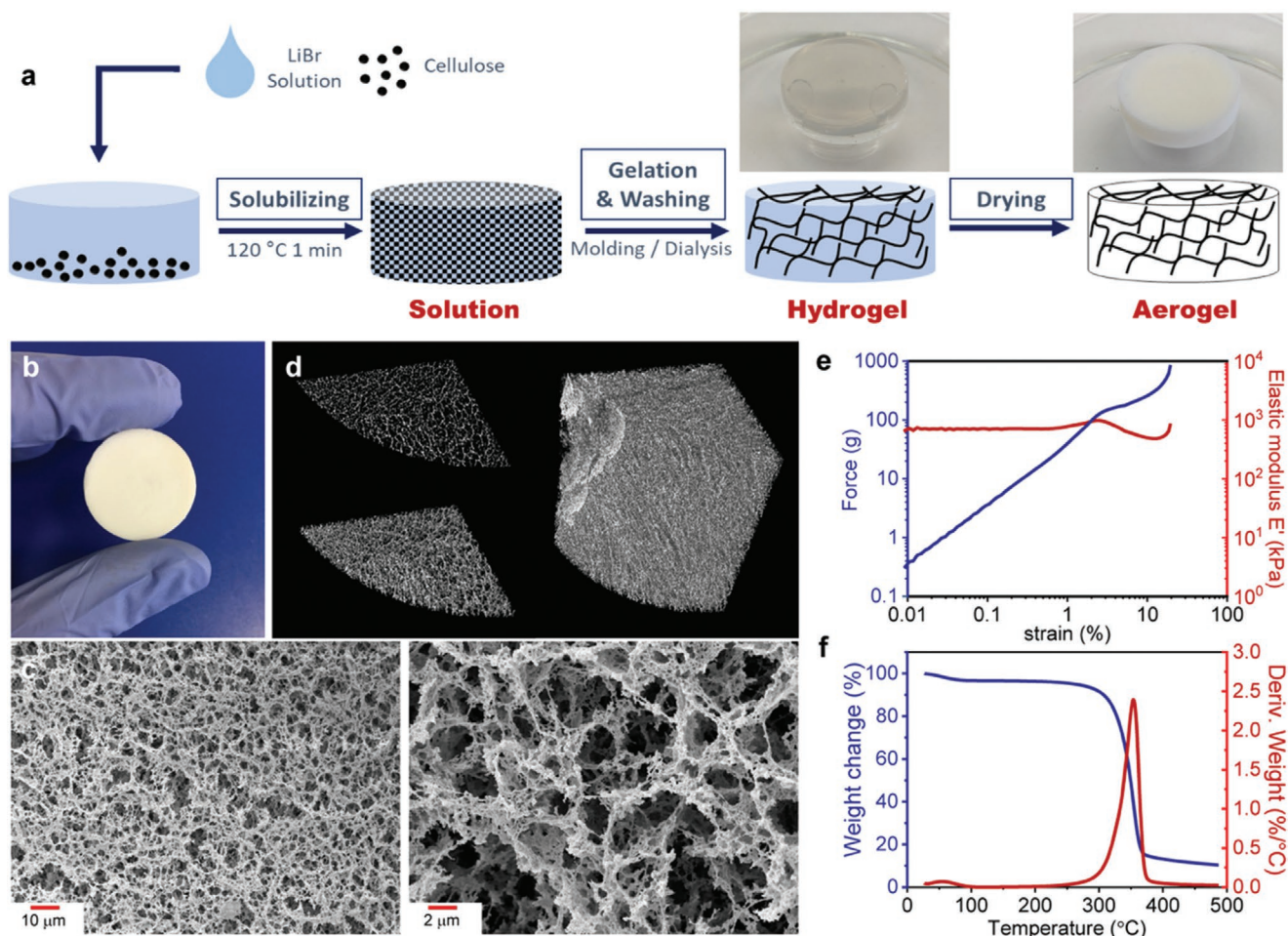


Figure 1. Fabrication process and characterization of the cellulose II network structured aerogel. a) Flow chart showing fabrication steps of cellulose II hydrogel and aerogel. b) Photograph of a well-shaped cellulose II aerogel. c) Scanning electron microscopic images of the aerogel cross section with different magnifications showing its uniform network structure and porous fiber surface. d) Layer-by-layer reconstruction of X-ray nano-computed tomography scan of the aerogel showing the interconnected open-pore 3D network structure. e) Dynamic strain sweep results of an 8 mm × 5 mm cellulose II aerogel cylinder under a testing frequency of 10 Hz. f) Thermogravimetric analysis of cellulose II aerogel.

2.2. Structure, Mechanism, and Characterization of the Cellulose II Aerogel-Based TENG

For application in energy harvesting TENG, a typical contact-separation mode was utilized in this study (Figure 2a). PTFE, one of the most commercially available triboelectric negative materials, was used as a reference material throughout all the measurements to evaluate the triboelectric performance of cellulose II aerogel. Two pieces of aluminum (Al) foil were, respectively, attached to both PTFE and cellulose II aerogel as back electrodes and connected to the external circuit for measuring the electric output.

Figure 2b shows the electricity-generation mechanism of cellulose II aerogel-based TENG. When applying a compressive force to the cellulose II aerogel-based TENG, charge transfer occurs based on the coupling effects of contact triboelectrification and electrostatic induction. Compared to a traditional film-based TENGs, the induced charges of the aerogel can not only exist on the contact surface but also distribute on the surface of structural network.^[10b,18] The unique nanostructure of the

cellulose II aerogel provides a large surface area and promotes the accumulation of charges due to the edge effect.^[18] When the force reverses, the increasing gap between the cellulose II aerogel and the PTFE separates the triboelectric charges with opposite polarities, thereby causing the increasing electric potential that drives the induced electrons flowing from the bottom electrode to the top electrode. The transient flow of electrons continues, which leads to instantaneous current flow through the external circuit, until an electrostatic equilibrium is achieved. When the force is re-applied on the TENG, the electrons backflow and form a current in the opposite direction. The periodic mechanical load-and-unload process makes the electrons flow back and forth through the external circuit.

To investigate the performance of cellulose II aerogel-based TENG for harvesting mechanical energy, a customized test setup was developed, as shown in Figure S2 (Supporting Information). During the electrical measurement, a linear motor that can control the applied forces via the stepping position was used, and the cellulose II aerogel was utilized with dimensions of 0.5 cm thickness and 2.8 cm diameter. The electrical voltage

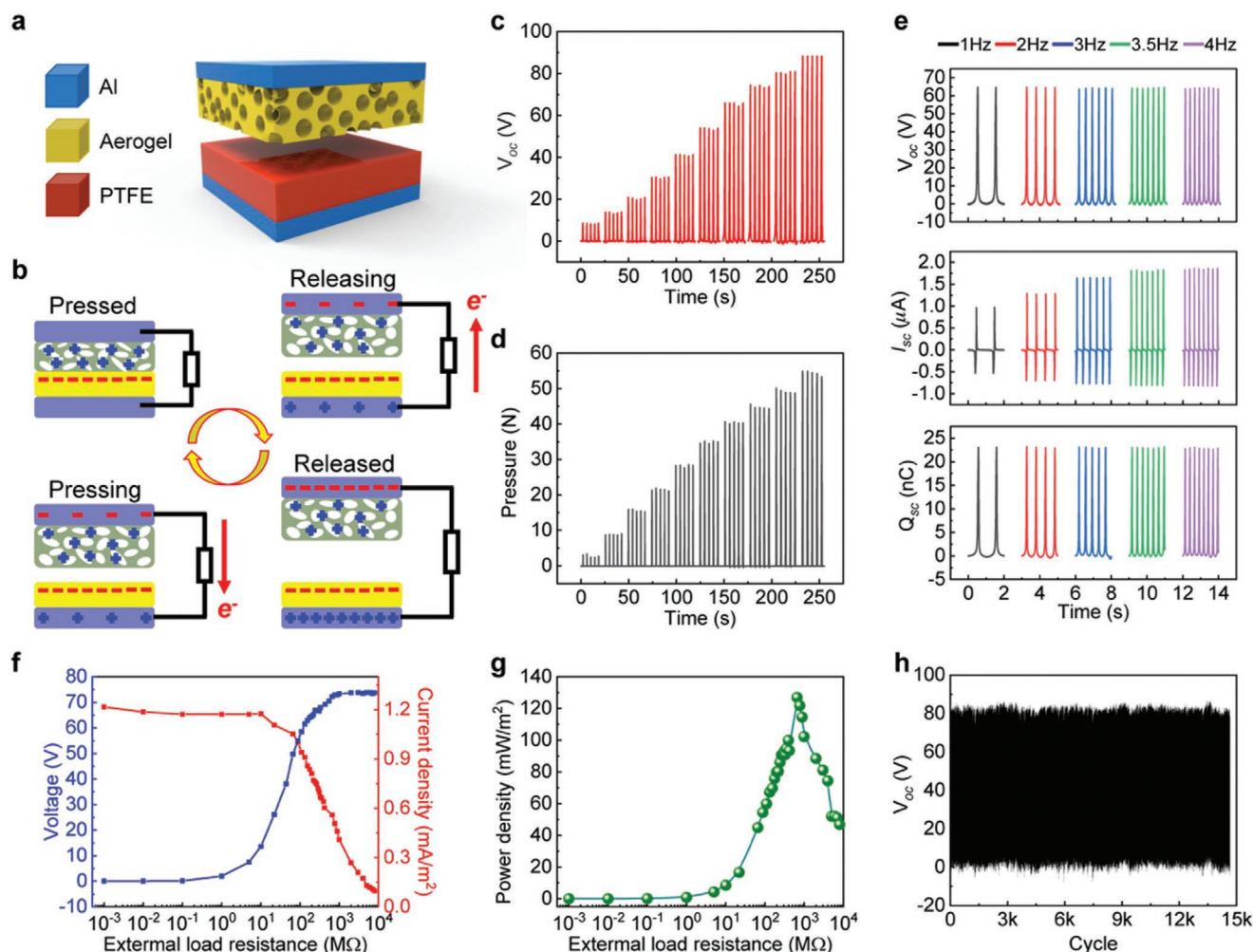


Figure 2. Structure, mechanism, and essential electrical characterization of the cellulose II aerogel-based TENG. a) Schematic of the layer-by-layer cellulose II aerogel-based TENG structure. b) Working mechanism of the cellulose II aerogel-based TENG. c,d) Mechanical response in terms of voltage output with different force values ranging from 2.4 to 54.4 N, and the corresponding sensitivity is 1.66 V N^{-1} . e) Open-circuit voltage, short-circuit current, and short-circuit charge under a 40 N force with different working frequency: 1, 2, 3, 3.5, and 4 Hz. f) Current density and voltage output under the different external load resistance. g) Dependence of output peak power density on the external load resistance as given by the expression $P = \frac{I^2 R}{S}$. h) Stability and durability test of the TENG performance for about 15 000 cycles. Note: the diameter of cellulose II aerogel in the measurement process is Φ 2.8 cm, and the corresponding area is 6.15 cm^2 calculated by $S = \pi r^2$.

output of the corresponding TENG increased linearly with the increasing applied force from 2.4 to 55 N (Figure 2c,d), corresponding to a sensitivity of 1.66 V N^{-1} , which was attributed to the greater contact area due to the increasing force.^[10b] Given the same applied force of 40 N, Figure 2e shows the results of open-circuit voltage (V_{oc}), short-circuit current (I_{sc}), and short-circuit charge (Q_{sc}) of the cellulose II aerogel-based TENG operating under various working frequencies (ranging from 1 to 4 Hz). Indistinct differences appeared in the V_{oc} ($\approx 65 \text{ V}$) and Q_{sc} ($\approx 23 \text{ nC}$) while the output peak value of the I_{sc} increased from 0.96 to $1.86 \mu\text{A}$ as the frequencies increased from 1 to 4 Hz.

Different external load resistances were also applied to evaluate the output performance of the cellulose II aerogel-based TENG (Figure 2f). With the increase in resistance from 1 k Ω to 10 G Ω at an operating frequency of 1 Hz, the peak output current density decreased while the peak output voltage exhibited a reverse trend. A maximum instantaneous power density of

127 mW m^{-2} was achieved at the load resistance of $\approx 660 \text{ M}\Omega$ (Figure 2g). The output power density P was calculated via $P = \frac{I^2 R}{S}$, where I denotes the output peak current across the external load, R denotes the load resistance, and S denotes the contact area of the cellulose aerogel and PTFE (6.15 cm^2 , calculated by $S = \pi r^2$). Durability is another critical factor for the energy harvesting device, which was tested using $\approx 15\,000$ cycles of periodic contact–separation events (Figure 2h). The open-circuit voltage of the TENG exhibited nearly unchanged, suggesting that the cellulose II aerogel-based TENG was robust.

2.3. Chemical and Physical Enhancement of Cellulose II Aerogel-Based TENG Performance

To further improve the performance of cellulose II aerogel-based TENG, we synthesized composite cellulose II aerogels

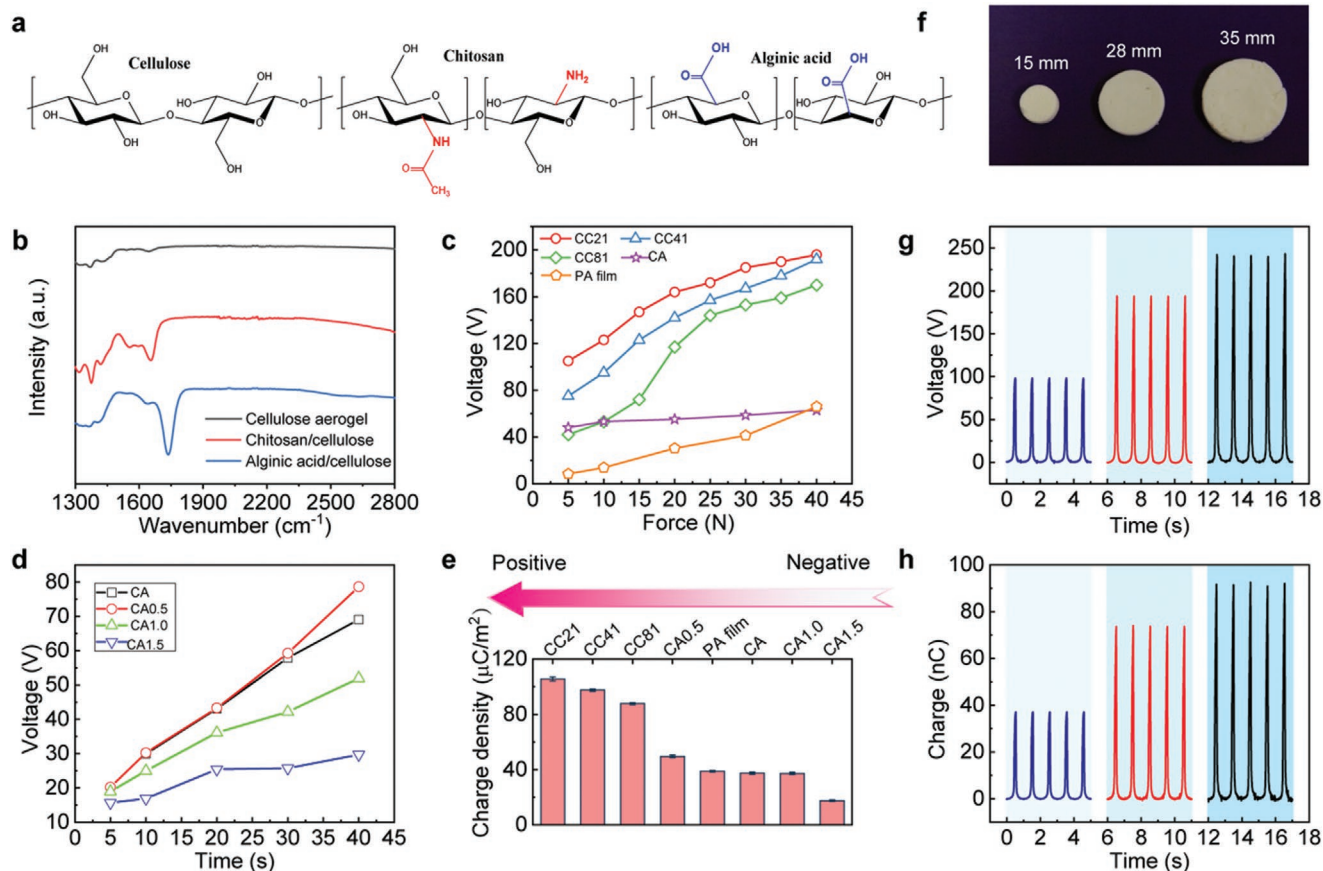


Figure 3. Chemically and physically tuned cellulose II composite aerogels for enhancing electrical performance of the corresponding TENGs. a) Chemical structures of cellulose, chitosan, and alginic acid. b) Fourier-transform infrared spectra of the pristine cellulose II aerogel, chitosan-composited cellulose II aerogel, and alginic acid-composited cellulose II aerogel. c) Comparison of the output voltage of the TENGs using pristine cellulose II aerogel (CA), cellulose aerogel with different chitosan content (from CC81 to CC21), and nylon (PA) film under different force values. d) Output voltage of the TENGs based on the cellulose II aerogel with different alginic acid contents (from CA0.5 to CA1.5), operating under different force values. e) The short-circuit charge density series using the PTFE as a reference layer under an applied force of 40 N. f) Physical image of the chitosan-composited CC21 cellulose II aerogels with different diameters, namely 15, 28, and 35 mm. g,h) Output open-circuit voltage and short-circuit charge of the TENGs based on samples with different areas under the same applied force of 40 N.

by introducing other natural polysaccharides, i.e., chitosan and alginic acid, which contain electron-donating and electron-withdrawing groups, respectively. **Figure 3a** shows the chemical structures of cellulose, chitosan, and alginic acid. Chitosan is produced from deacetylating chitin. Pure chitosan is composed of β -(1,4)-linked D-glucosamine, but commercial chitosan usually contains randomly distributed N-acetyl-D-glucosamine due to incomplete deacetylation. The degree of deacetylation of the chitosan used in this study was 82.4%, determined from the quantity of acetic acid released from the hydrolysis of acetyl groups, suggesting that most (82.4%) of the structural units of the chitosan had free amine groups, which can potentially serve as strong electron-donating groups. Alginic acid is a linear polymer composed of two structural units, namely β -D-mannuronate and its epimer α -L-guluronate. They are linked by β -(1,4)-bond, and both have a carboxylic acid group per unit, which can serve as electron-withdrawing groups. The Fourier transform infrared (FTIR) spectra of the prepared cellulose–chitosan, cellulose–alginic acid composite aerogels, and the pristine cellulose II aerogel are shown in **Figure 3b**. The small peak

at the wavenumber of 1630 cm^{-1} is from the absorbed moisture caused by the highly hydrophilic hydroxyl group, which appears in all three aerogels. For cellulose–chitosan composite aerogel, the peak at the wavenumber of 1660 cm^{-1} originates from the N–H stretching vibration and oscillations of C=O in amide groups, known as the amide I peak. The peak at 1550 cm^{-1} is a typical amide II peak of secondary amide. Both peaks verified the presence of acetylamino groups in the cellulose–chitosan composite aerogel. Similarly, the cellulose–alginic acid aerogel exhibits a typical large COOH peak at 1740 cm^{-1} . These results reveal that the desired electron-donating and electron-withdrawing functional groups were introduced homogeneously into the composite aerogels.

Figure 3c presents the output voltage of the cellulose–chitosan aerogel-based TENGs prepared by using aerogels with different chitosan contents. For easy description, the cellulose–chitosan composite aerogels with the cellulose-to-chitosan mass ratios of 2:1, 4:1, 8:1, and 1:0 are named as CC21, CC41, CC81, and CA, respectively. Nylon film (PA), which is known of having excellent triboelectric positive property, was paired with PTFE as

a control experimental setup. When the applied force increased from 5 to 40 N, the output voltage of paired nylon/PTFE-based TENG slightly increased from 47 to 63 V. The pristine cellulose II aerogel-based TENG (CA/PTFE) exhibited lower output performance of 8 V under the force of 5 N. However, the output voltages of such device increased to 63 V, which was identical to that of the nylon/PTFE-based TENG, under 40 N stress. This demonstrated the excellent sensitivity of the aerogel II-based TENG with respect to the applied force, compared to film based TENGs like nylon and PTFE-based one.^[19] Moreover, increasing chitosan content in the cellulose–chitosan composite aerogels significantly enhanced the electrical voltage output of corresponding devices from 269% (CC81) to 311% (CC21), compared to that of the pristine cellulose II aerogel (CA)-based and nylon film (PA)-based devices under with the same stress of 40 N. Under different working frequencies, as shown in Figure S3 (Supporting Information), the short-circuit current output of CC21-based TENG exhibits a similar output improvement, which further confirms the excellent performance of the cellulose–chitosan composite aerogels. On the other hand, the cellulose–alginate aerogel-based TENGs—with the increasing content of alginate acid from 0% to 1.5% (named as CA, CA0.5, CA1.0, and CA1.5)—exhibited an opposite trend, as alginate acid provides more electron-withdrawing groups, unlike the electron-donating groups in chitosan. For example, the voltage of the CA1.5-based TENG showed a 43% retention compared to that of the pristine CA-based TENG, suggesting the enhanced performance toward the triboelectric negative direction, owing to PTFE, a triboelectric negative material as reference material, as shown in Figure 3d. These observations indicated that the amino-group-enriched chitosan and carboxyl-group-enriched alginate acid shifted the triboelectric performance in opposite directions. The corresponding short-circuit charge density changed from $175 \mu\text{C m}^{-2}$ (CA1.5) to $105.7 \mu\text{C m}^{-2}$ (CC21), when PTFE is used as another triboelectric layer in the corresponding TENGs, as shown in Figure 3e, which consolidates the speculation.

It was observed that the electrical output of the TENGs intuitively depended on the physical dimensions of the cellulose aerogels. A couple of additional key features of our aerogel preparation method are that the production of cellulose II aerogel can be easily scaled up and customized with complicated shapes. When the diameter of the CC21 samples increased from 15 to 35 mm (Figure 3f), the output voltage and charge of the corresponding TENGs were significantly enhanced, as shown in Figure 3g,h. Specifically, CC21-based TENGs with diameters of 15, 28, and 35 mm generated V_{oc} values of 98, 196, and 242 V, and Q_{sc} values of 37, 74, and 92 nC, respectively. The electrical output of the cellulose II aerogel-based TENGs that are fabricated by different types of aerogels with or without mechanical compression prior to the measurement is shown in Figure S4 (Supporting Information). The electric outputs of the TENGs made of precompressed aerogels were lower than that of the TENGs made of the non-precompressed, same type of aerogels. Without the precompression, the aerogels are expected to encounter larger strains when external forces are applied. The result implies that more significant mechanical strain can potentially promote more inner induced charge transfer, resulting in higher electrical outputs. Moreover, we also evaluated how the thickness of cellulose II aerogel can affect the electric output of the corresponding TENGs. The electric outputs of the pristine cellulose II aerogel-based TENG and

CC21-based TENG with different aerogel thicknesses are exhibited in Figure S5 (Supporting Information). Table S1 (Supporting Information) also presents the detailed information for those aerogel samples. As can be seen from Figure S5 (Supporting Information), the experimental results reveal that increasing the thickness of the porous aerogels, the corresponding output performance of such TENGs can be improved.

2.4. Applications of Cellulose II Aerogel-based TENG

To validate the capacity of harvested mechanical energy, for example, the energy of human motions, in practical applications, we fabricated an independent cellulose II aerogel-based TENG (CC21), as shown in Figure 4a. By tapping the cellulose II aerogel-based TENG with a finger, the device was able to illuminate 60 green light-emitting diodes (LEDs) connected in series and the patterned “AG” letter-shaped LEDs (Figure 4b,c; Movies S1 and S2, Supporting Information). Energy storage devices, such as a capacitor, can be used to store the electrical energy harvested from the cellulose II aerogel-based TENG for subsequent use. We investigated the effect of capacitance (0.22–22 μF) and working frequency (1–8 Hz) on the charging performance of the cellulose II aerogel-based TENG (Figure 4d,e). The results show that the capacitors were charged faster as capacitors with smaller capacitance or it was operating at a higher working frequencies. Besides, the electrical energy harvested by the cellulose II aerogel-based TENG and stored in the capacitor can be utilized to power a commercial calculator, as shown in Figure 4f and Movie S3 (Supporting Information). By connecting with the electric circuit shown in the inset of Figure 4f, the calculator functioned when the charging voltage reached the rated value of 1.5 V. This process of charging to 1.5 V only took ≈ 3 s. Subsequently, the calculator functioned continuously in a stable manner. All the demonstrations above indicate that the cellulose II aerogel-based TENG provided sufficient power for operating many portable electronics, thus, suggesting that it can potentially serve as a green sustainable power source.

We further demonstrated a potential application of cellulose II aerogel-based TENG in a self-powered sensor. A round-shaped cellulose II aerogel sample (CC21 with a diameter of 28 mm) was taped on a sock for wearable motion monitoring (Figure 4g). The contact between the heel and ground would generate evident electrical output. Given the thin thickness (5 mm) and excellent mechanical flexibility of the cellulose II aerogel, it would barely change the gait of the wearer. Additionally, the porous network of the aerogel can potentially endow the wearer with increased breathability. In the demonstration, two typical motions, namely walking and running, were performed. The current outputs with different amplitudes and distinct signal styles were obtained, as shown in Figure 4h,i. Both curves exhibit periodic alternating current (AC) characteristics, which include two parts: namely, the upper part of an AC signal resulting from the contact of the two layers and the bottom part that is due to the separation process between the feet and ground. In the case of running, the current output of the cellulose aerogel-based TENG is higher ($\approx 1 \mu\text{A}$) compared to the output resulting from walking process (0.5 μA), which is attributed to the higher motion frequency of running (≈ 2 Hz) compared to the lower frequency of walking (about 1 Hz).

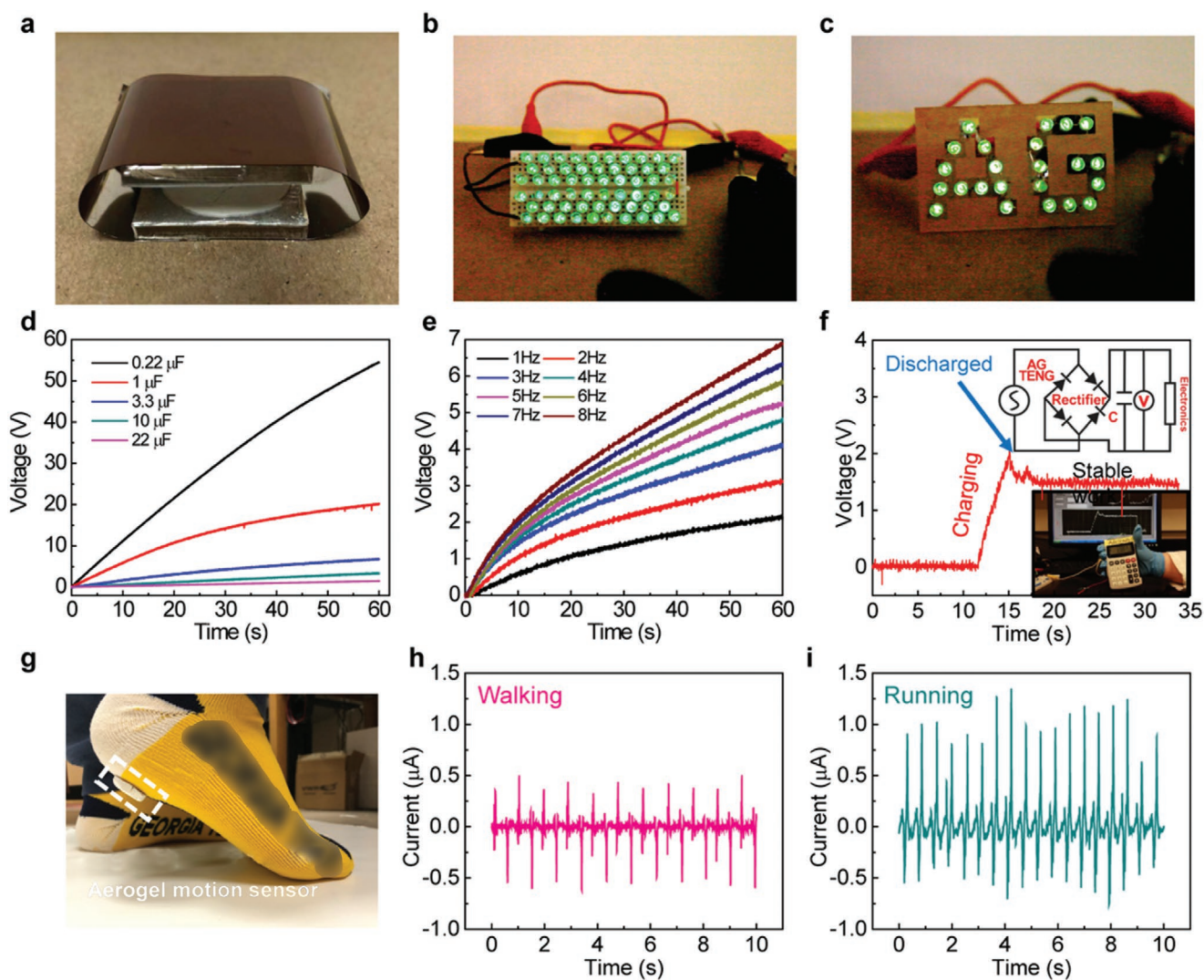


Figure 4. Applications of harvesting mechanical energy, powering portable electronics, and self-powered motion monitoring using cellulose II aerogel-based TENGs. a) An independent contact–separation mode cellulose II aerogel-based TENG device (CC21, Φ : 28 mm, area: 6.15 cm²). b,c) Demonstrations of lighting up 60 LEDs and the “AG” pattern by the cellulose II aerogel-based TENG using finger pressing. Charging capability of the cellulose II aerogel-based TENG d) using capacitors with different capacitance values (0.22–22 μ F) and e) different working frequencies (1–8 Hz). f) Demonstrations of powering a commercial calculator and the charging voltage curve as a function of charging time. Inset: the electric circuit of the charging system. g) Photograph of the cellulose II aerogel-based TENG attached on a sock. h,i) Current signals during the process of walking and running for real-time human motion monitoring.

It is worth noting that when compared with traditional synthetic polymer-based and cellulose I-based TENG, the cellulose II aerogel-based TENG has several advantages. First, the highly porous aerogel structure endows the corresponding TENGs with higher mechanical response sensitivity and better electrical output performance likely because of the increased surface area and the charge density as mentioned above. In addition, the process of introducing electron-donating and electron-withdrawing groups is easy that can tune the cellulose II aerogel with different triboelectric polarities to further improve the performance of the resultant TENGs. Furthermore, cellulose, chitosan, and alginate are all cost effective, abundant, and sustainable natural polysaccharides. Thus, the cellulose II aerogels in alliance with TENG lead to a more promising system for applications in biomechanical energy harvesting and self-powered health monitoring. Nevertheless, the proposed cellulose II aerogel-based

TENG, which is still in its early stage, exhibits great potential. For future research, additional natural polymers with different functional groups could be readily introduced into the composite aerogels to explore different triboelectric performance. Also, cellulose II aerogel-based TENGs with different working modes and functions can be designed for various applications.

3. Conclusion

In summary, the cellulose II aerogel-based TENG is reported for the first time in this study as a mechanical energy harvester and self-powered sensor. Cellulose II aerogels were fabricated via a dissolution–regeneration process in a green solvent, lithium bromide trihydrate (a molten salt hydrate). The prepared cellulose II aerogel had an interconnected open-pore

3D network structure, more flexible property, extremely high porosity, and large surface area. The implemented cellulose II aerogel-based TENG achieved high electrical performance and excellent mechanical response sensitivity. Composite cellulose II aerogels with chitosan and alginate were fabricated to further improve the performance of the corresponding TENGs. The introduced electron-donating and electron-withdrawing groups (NH_2 from chitosan and COOH from alginate, respectively) enhanced the electrical performance of the composited aerogel-based TENGs compared to that of the pristine cellulose II aerogel-based device. We successfully demonstrated potential applications of the cellulose II aerogel-based TENG in powering commercial LEDs and a portable calculator, and in monitoring human motion pattern, such as walking or running. The study demonstrated not only the fabrication of cellulose II aerogels but also the development of a green and high-performance energy harvesting and self-powering system.

4. Experimental Section

Fabrication of Cellulose II Aerogel: For cellulose II aerogel, 0.06 g of microcrystalline cellulose (Avicel PH-101, Sigma-Aldrich, St. Louis, MO) was added into a glass vial with 6 g of 60% wt/wt LiBr (Alfa Aesar, Ward Hill, MA) solution (1 wt% cellulose in LiBr solution). The glass vial was immersed into a glycerol bath at 120 °C for 1 min with magnetic stirring to solubilize cellulose fully. Subsequently, the clear solution was poured into a pyrex 20 mL beaker (with an inner diameter of 30 mm) and cooled to room temperature. During the cooling process, gelation occurred, and the liquid solution became a soft matter with a cylindrical shape. Washing the soft matter with excessive water to completely replace LiBr and regenerate cellulose gave a hydrogel. Then, the water in the hydrogel was exchanged to ethanol then *tert*-butanol, and after freeze-drying aerogel was fabricated. The resultant aerogel was a regular cylinder with a diameter of 28 mm and a height of 5 mm.

Fabrication of Cellulose–Chitosan Composite Aerogel: Cellulose–chitosan composite aerogels were fabricated with different mass ratios of chitosan (medium molecular weight, Sigma-Aldrich, St. Louis, MO) to cellulose (1:2, 1:4, and 1:8, respectively). The total mass of cellulose and chitosan was 0.06 g to maintain 1 wt% total mass in the LiBr solution. The chitosan was first added into the 60% LiBr solution and solubilized at 140 °C for 10 min. Subsequently, the cellulose was added, dispersed, and solubilized in additional 5 min. The resultant clear solution was poured into a 20 mL beaker and cooled to room temperature to get a soft matter and then the final aerogel by following the same procedure as that for the pure cellulose aerogel above.

Fabrication of Cellulose–Alginate Composite Aerogel: For cellulose–alginate composite aerogel, cellulose hydrogels with 0.75 wt% cellulose in 60 wt% LiBr solution were prepared following the same procedure as described above. The resultant hydrogels were soaked in 0.5, 1, and 1.5 wt% sodium alginate solutions with sonication for 2 h, respectively. The treated hydrogels were then immersed into 0.1 M HCl solution to precipitate alginate. Excessive water was then used to wash off HCl until the pH became 7. The subsequent solvent exchange and drying procedures were the same as above.

Assembly of Cellulose II Aerogel-Based TENGs: All TENGs used in the study were of the typical vertical contact–separation mode. The schematic diagram of the measurement setup is shown in Figure S2 (Supporting Information). Briefly, a fixed part was constructed by sandwiching an Al foil between a PTFE film and acrylic substrate. The thickness of PTFE was $\approx 125 \mu\text{m}$. The movable part of TENG was constructed by attaching an Al foil and cellulose II aerogel successively to the acrylic board. The movable part was mounted

on a linear motor, and another part was fixed facing each other on a manually controllable displacement stage including a force sensor. The linear motor moves the movable part with a displacement of 30 mm, a speed of 0.06 m s^{-1} , and an acceleration of 5 m s^{-2} without any waiting time. The displacement stage was utilized to accurately control the applied pressure. The operating frequency could be adjusted by changing the operating parameters of linear motor mentioned above.

Aerogel Characterization: The SEM images were obtained using an LEO 1530 scanning electronic microscope (Leo Co., Oberkochen, Germany) with a 3 kV electron gun voltage. The continuous 3D structure of the cellulose aerogels was obtained using a high-resolution X-ray nano-computed tomography scanner (SkyScan 2211, Bruker, Billerica, MA) equipped with a 190 kV/50 μA to 1 mA X-ray source and an 11 megapixel (4000×2600) X-ray sensitive CCD camera. The samples were scanned using an accelerating voltage of 50 kV, a target current of 180 μA , a 0.1 μm tungsten source target, a full 360° sample rotation (0.20° increment), and an exposure time of 100 ms per frame. Reconstruction was performed using Bruker CTvox software.

The mechanical analysis was conducted using an RSA III dynamic mechanical analyzer (TA Instruments, New Castle, DE). The dynamic strain sweep test at room temperature was performed in the compression mode on 8 mm parallel plates (Figure S1, Supporting Information). To fit the testing parallel plates, the gels were shaped into cylinders of 8 mm (diameter) \times 5 mm (thickness) using a 2 mL microcentrifuge tube as a mold.

The specific surface area of aerogel was measured via nitrogen adsorption–desorption analysis at $-196 \text{ }^\circ\text{C}$ (Gemini VII 2390, Micromeritics, Norcross, GA). Aerogel samples were first degassed at 110 °C overnight on a sample preparation system (VacPrep 061, Micromeritics, Norcross, GA) to remove moisture. The Brunauer–Emmett–Teller specific surface area and Barrett–Joyner–Halenda pore size distribution were calculated using the Gemini VII software from the obtained isotherms. Thermal stability of the aerogel was tested using a Q500 thermogravimetric analyzer (TA Instruments, New Castle, DE) in a nitrogen atmosphere from 25 to 500 °C. Fourier transform infrared spectroscopy was performed using a Perkin Elmer spectrum 100 FT-IR spectrometer (Perkin Elmer, Waltham, MA).

Degree of Deacetylation of Chitosan: The chitosan was treated with sulfuric acid to release acetyl groups from the amine position as acetic acid. Acetic acid released was quantitated via high-performance liquid chromatography on a Dionex ICS-3000 system equipped with a Supelcogel C-610H column ($7.8 \times 300 \text{ mm}$) at 30 °C and a UV detector at 210 nm. An isocratic flow of 0.1% phosphoric acid was used as the mobile phase at 0.6 mL min^{-1} .^[20] The degree of deacetylation of chitosan was calculated from the quantity of acetyl groups.

Electrical Characterization: The electrical output was measured using a programmable electrometer (Keithley 6514) and recorded using a program written using Labview. Informed signed consent was obtained from the volunteers for the tests.

Supporting Information

Supporting Information is available from the Wiley Online Library or from the author.

Acknowledgements

L.Z., Y.L., and Y.-C.W. contributed equally to this work. The authors gratefully acknowledge the support of the Hightower Chair foundation of the Georgia Institute of Technology, the support of the Sichuan Science and Technology Program (Program No. 2018RZ0074), and the support of U.S. Department of Agriculture (USDA) National Institute of Food and Agriculture (NIFA) McIntire Stennis project (WIS01996).

Conflict of Interest

The authors declare no conflict of interest.

Keywords

energy harvesting, human motion monitoring, regenerated cellulose, self-powered sensors, triboelectric nanogenerators

Received: February 24, 2020

Revised: April 8, 2020

Published online:

-
- [1] L. Zhang, B. Zhang, J. Chen, L. Jin, W. Deng, J. Tang, H. Zhang, H. Pan, M. Zhu, W. Yang, *Adv. Mater.* **2016**, *28*, 1650.
- [2] L. Zhang, L. Jin, B. Zhang, W. Deng, H. Pan, J. Tang, M. Zhu, W. Yang, *Nano Energy* **2015**, *16*, 516.
- [3] a) X. J. Zhao, S. Y. Kuang, Z. L. Wang, G. Zhu, *ACS Nano* **2018**, *12*, 4280; b) S. L. Zhang, M. Xu, C. Zhang, Y.-C. Wang, H. Zou, X. He, Z. Wang, Z. L. Wang, *Nano Energy* **2018**, *48*, 421.
- [4] a) B. Zhang, L. Zhang, W. Deng, L. Jin, F. Chun, H. Pan, B. Gu, H. Zhang, Z. Lv, W. Yang, *ACS Nano* **2017**, *11*, 7440; b) S. L. Zhang, Y. C. Lai, X. He, R. Liu, Y. Zi, Z. L. Wang, *Adv. Funct. Mater.* **2017**, *27*, 1606695; c) S. L. Zhang, Q. Jiang, Z. Wu, W. Ding, L. Zhang, H. N. Alshareef, Z. L. Wang, *Adv. Energy Mater.* **2019**, *9*, 1900152.
- [5] a) Z. L. Wang, A. C. Wang, *Mater. Today* **2019**, *30*, 34; b) Z. L. Wang, *Mater. Today* **2017**, *20*, 74.
- [6] Z. L. Wang, *Nano Energy* **2019**, *58*, 669.
- [7] a) H. Sai, R. Fu, L. Xing, J. Xiang, Z. Li, F. Li, T. Zhang, *ACS Appl. Mater. Interfaces* **2015**, *7*, 7373; b) A. Mulyadi, Z. Zhang, Y. Deng, *ACS Appl. Mater. Interfaces* **2016**, *8*, 2732; c) N. Islam, S. Li, G. Ren, Y. Zu, J. Warzywoda, S. Wang, Z. Fan, *Nano Energy* **2017**, *40*, 107.
- [8] a) A. Chandrasekhar, N. R. Alluri, B. Saravanakumar, S. Selvarajan, S.-J. Kim, *J. Mater. Chem. C* **2017**, *5*, 1810; b) J. Peng, H. Zhang, Q. Zheng, C. M. Clemons, R. C. Sabo, S. Gong, Z. Ma, L. S. Turng, *Nanoscale* **2017**, *9*, 1428; c) B. Chen, N. Yang, Q. Jiang, W. Chen, Y. Yang, *Nano Energy* **2018**, *44*, 468; d) H.-J. Kim, E.-C. Yim, J.-H. Kim, S.-J. Kim, J.-Y. Park, I.-K. Oh, *Nano Energy* **2017**, *33*, 130.
- [9] A. Du, B. Zhou, Z. H. Zhang, J. Shen, *Materials* **2013**, *6*, 941.
- [10] a) C. Yao, A. Hernandez, Y. Yu, Z. Cai, X. Wang, *Nano Energy* **2016**, *30*, 103; b) Q. Zheng, L. Fang, H. Guo, K. Yang, Z. Cai, M. A. B. Meador, S. Gong, *Adv. Funct. Mater.* **2018**, *28*, 1706365.
- [11] a) Y. Zi, H. Guo, Z. Wen, M.-H. Yeh, C. Hu, Z. L. Wang, *ACS Nano* **2016**, *10*, 4797; b) S. Niu, Z. L. Wang, *Nano Energy* **2015**, *14*, 161; c) X. S. Meng, Z. L. Wang, G. Zhu, *Adv. Mater.* **2016**, *28*, 668; d) C. Jia, D. Wenbo, Z. Yunlong, L. Yijia, J. Linhong, L. Fan, W. Changsheng, W. Z. Lin, *Nat. Commun.* **2018**, *9*, 3733; e) P. Jiang, L. Zhang, H. Guo, C. Chen, C. Wu, S. Zhang, Z. L. Wang, *Adv. Mater.* **2019**, *31*, 1902793; f) K. Chen, L. Zhang, X. Kuang, V. Li, H. J. Qi, *Adv. Funct. Mater.* **2019**, *29*, 1903568.
- [12] B. Lindman, G. Karlström, L. Stigsson, *J. Mol. Liq.* **2010**, *156*, 76.
- [13] S. Sen, J. D. Martin, D. S. Argyropoulos, *ACS Sustainable Chem. Eng.* **2013**, *1*, 858.
- [14] a) L. Shuai, X. Pan, *US Patent 9,487,712B2*, **2016**; b) X. Pan, L. Shuai, *US Patent 9,187,790B2*, **2015**.
- [15] a) Y. J. Yang, J. M. Shin, T. H. Kang, S. Kimura, M. Wada, U. J. Kim, *Cellulose* **2014**, *21*, 1175; b) Y. Liao, Z. Pang, X. Pan, *ACS Sustainable Chem. Eng.* **2019**, *7*, 17723.
- [16] J. Rouquerol, D. Avnir, C. W. Fairbridge, D. H. Everett, J. H. Haynes, N. Pernicone, J. D. F. Ramsay, K. S. W. Sing, K. K. Unger, *Pure Appl. Chem.* **1994**, *66*, 1739.
- [17] a) X. Yang, K. Shi, I. Zhitomirsky, E. D. Cranston, *Adv. Mater.* **2015**, *27*, 6104; b) Y. Xuan, E. D. Cranston, *Chem. Mater.* **2014**, *26*, 6016.
- [18] a) K. Y. Lee, J. Chun, J. H. Lee, K. N. Kim, N. R. Kang, J. Y. Kim, M. H. Kim, K. S. Shin, M. K. Gupta, J. M. Baik, S. W. Kim, *Adv. Mater.* **2014**, *26*, 5037; b) C. Xu, L. Zhang, Y. Xu, Z. Yin, Q. Chen, S. Ma, H. Zhang, R. Huang, C. Zhang, L. Jin, *J. Mater. Chem. A* **2017**, *5*, 189.
- [19] a) S. Niu, S. Wang, L. Lin, Y. Liu, Y. S. Zhou, Y. Hu, Z. L. Wang, *Energy Environ. Sci.* **2013**, *6*, 3576; b) S. H. Wang, L. Lin, Y. N. Xie, Q. S. Jing, S. M. Niu, Z. L. Wang, *Nano Lett.* **2013**, *13*, 2226.
- [20] L. Shuai, Q. Yang, J. Y. Zhu, F. C. Lu, P. J. Weimer, J. Ralph, X. J. Pan, *Bioresour. Tech.* **2010**, *101*, 3106.